JOURNAL OF THE ROYAL SOCIETY Interface

CrossMark click for updates

J. R. Soc. Interface (2012) **9**, 2735–2744
doi:10.1098/rsif.2012.0286
Published online 6 June 2012

Strain amplification in bone mechanobiology: a computational investigation of the *in vivo* mechanics of osteocytes

Stefaan W. Verbruggen, Ted J. Vaughan and Laoise M. McNamara*

Biomechanics Research Centre (BMEC), Mechanical and Biomedical Engineering, College of Engineering and Informatics, National University of Ireland, Galway, Republic of Ireland

The osteocyte is believed to act as the main sensor of mechanical stimulus in bone, controlling signalling for bone growth and resorption in response to changes in the mechanical demands placed on our bones throughout life. However, the precise mechanical stimuli that bone cells experience *in vivo* are not yet fully understood. The objective of this study is to use computational methods to predict the loading conditions experienced by osteocytes during normal physiological activities. Confocal imaging of the lacunar–canalicular network was used to develop three-dimensional finite element models of osteocytes, including their cell body, and the surrounding pericellular matrix (PCM) and extracellular matrix (ECM). We investigated the role of the PCM and ECM projections for amplifying mechanical stimulation to the cells. At loading levels, representing vigorous physiological activity (3000 $\mu\varepsilon$), our results provide direct evidence that (i) confocal image-derived models predict 350–400% greater strain amplification experienced by osteocytes compared with an idealized cell, (ii) the PCM increases the cell volume stimulated more than 3500 $\mu\varepsilon$ by 4–10% and (iii) ECM projections amplify strain to the cell by approximately 50–420%. These are the first confocal image-derived computational models to predict osteocyte strain *in vivo* and provide an insight into the mechanobiology of the osteocyte.

Keywords: bone; osteocyte; mechanobiology; lacuna; pericellular matrix; tissue strain

1. INTRODUCTION

Bone is a dynamic and adaptive material that can continuously adapt its mass and structure to meet the mechanical demands experienced throughout life. This adaptive behaviour is fundamental to physiological function as it allows the skeleton to survive under the variety of loading conditions experienced throughout life. The exact nature of how bone can detect and communicate the need for bone repair is unknown. It has been shown that bone cells, such as osteoblasts and osteocytes, are capable of transducing mechanical signals into biochemical stimuli [1]. Osteocytes have long been regarded to be the primary mechanosensors of bone, owing to their ubiquitous spatial distribution throughout bone and their extensive communication network facilitated by cell processes that extend to other osteocytes and osteoblasts. It is believed that these cells act as a network of strain gauges that monitor the mechanical environment, and direct and recruit other cells to adapt bone mass when mechanical demands are altered. Recent studies have suggested the pathogenesis of bone diseases may be correlated to the mechanobiology of bone cells [2] and that mechanical stimulation enhances bone tissue regeneration *in vitro* to a certain extent [3,4], although the precise mechanisms by which mechanical stimulation can enhance regeneration is not yet fully understood. It is likely that mechanobiology-based approaches for bone tissue regeneration would be enhanced if levels of mechanical stimulation applied to cells *in vitro* were analogous to those experienced *in vivo*. However, the precise mechanical stimuli that bone cells experience *in vivo*, and the mechanical stimuli that initiate a biochemical response are not fully understood.

It is well accepted that bone requires regular loading to remain healthy. Burr *et al.* [5] and Fritton *et al.* [6] have quantified these strains, observing that whole bones routinely experience mechanical strains between 1000 and 2000 $\mu\varepsilon$. It is believed that disuse bone resorption is initiated less than 1000 $\mu\varepsilon$, whereas it has been observed that vigorous exercise generates strains up to 3000 $\mu\varepsilon$ and stimulates new bone formation. Furthermore, strains more than 3500 $\mu\varepsilon$ lead to damage and resorption of bone [7], with fracture of bone occurring more than 4000 $\mu\varepsilon$ [8]. However, this presents a

*Author for correspondence (laoise.mcnamara@nuigalway.ie).

Received 5 April 2012
Accepted 4 May 2012

paradox, as cell culture studies have shown that *in vitro* osteoblasts and osteocytes do not generate a biochemical response to levels of strain approximately less than 5000 $\mu\varepsilon$, with an appreciable response occurring only approximately more than 10 000 $\mu\varepsilon$ [9,10]. This would suggest that some form of strain amplification occurs during strain transfer to the osteocyte *in vivo*, as the strains necessary to elicit an osteogenic response from cells would damage the extracellular bone matrix. Investigation of this strain amplification effect is critical to understand bone cell mechanobiology.

As osteocytes are embedded in a mineralized, matrix direct experimental studies of these cells within their native environment are challenging. A particular challenge to understand the mechanical environment surrounding bone cells has been the difficulty in obtaining information regarding the geometry of osteocytes *in situ*. At present, high-resolution imaging of the osteocyte environment under mechanical loading has been limited to two-dimensional imaging of sections through the lacunae on an exposed optical microscopy plane [11–14]. Using these methods, it has been observed that large variations in perilacunar strain exist, with average strains between 7500 and 20 000 $\mu\varepsilon$, and peak strains as high as 35 000 $\mu\varepsilon$, under an applied load of 2000 $\mu\varepsilon$.

Researchers have sought to overcome experimental challenges by developing idealized theoretical models of osteocyte canaliculi and predicted the approximate levels of shear stress (0.8–3 Pa) at the cell membrane under load-induced fluid flow [15–18]. In particular, these studies have shown that load-induced fluid drag on the pericellular matrix (PCM) might amplify the strain experienced at the cell membrane to levels that initiate a biochemical response [15,17]. Recent studies, using a novel fixation technique and transmission electron microscopy (TEM), also revealed the presence of localized projections of the extracellular matrix (ECM) into the pericellular space of the canaliculi in which osteocyte cell processes are located [19]. As it has been demonstrated that the cell processes of osteocytes are the most mechanosensitive parts of the cell, with a highly developed actin cytoskeleton throughout, these projections may play a critical role in strain amplification [20]. Indeed, theoretical models have shown that ECM projections magnify the axial loading experienced by the cell by an order of magnitude more than the radial strain generated by transverse tethering elements in the PCM [21].

Computational modelling has also been used as a tool to characterize the osteocyte mechanical environment. A three-dimensional idealized finite element model of a whole osteocyte lacuna was developed and predicted that a strain amplification factor of 1.26–1.52 occurred for an applied global strain of 2000 $\mu\varepsilon$, increasing to 3 with the inclusion of canaliculi in the simulations [22]. However, both the analytical studies and this computational approach employed idealized geometries, which do not accurately represent osteocytes *in vivo*. Computational fluid dynamic models of individual canaliculi were developed using three-dimensional axisymmetric models generated from two-dimensional TEM images of osteocyte canaliculi and have predicted that the canalicular geometry has a profound effect on shear stress experienced by cell process under interstitial fluid flow [23]. However, the lacunar and cell body geometry were not included in these models and, whereas the role of fluid flow was considered, direct mechanical stimulation of the osteocyte by the surrounding matrix components was not investigated. Therefore, detailed geometrically accurate models are fully required to understand the role of the complex three-dimensional geometry of the lacunar–canalicular network on the mechanical stimulation experienced by osteocytes under physiological loading. Some attempts have been made to develop computational models of osteocyte lacunae from three-dimensional reconstructions of confocal images [24], but these did not include the cellular or pericellular components and predicted perilacunar strains only, not strains experienced by osteocytes.

The objectives of this research are (i) to develop solid models of osteocytes that closely represent their geometry *in vivo* and (ii) to use computational methods to predict the loading conditions experienced by osteocytes during normal physiological activities. We develop confocal image-derived models of an osteocyte and its immediate surroundings. These studies are compared with the idealized models of osteocytes to examine the effect of confocal image-derived geometries on strain predicted in the cell. We also investigate the role of the PCM and ECM projections as strain amplifiers in osteocyte mechanobiology.

2. MATERIAL AND METHODS

2.1. Confocal imaging of osteocytes

To visualize osteocytes within their native environment, fluorescent staining of the lacunar–canalicular space and confocal imaging were performed. Thick transverse sections (400 μm) of the tibia of a male, six- to eight-month-old Sprague–Dawley rat were cut using a diamond blade saw (Isomet, Buehler) and then fixed in 4 per cent paraformaldehyde for 24 h at room temperature. Sections were then dehydrated in ascending graded ethanol (75%, 95% and 100%, 5 min each). These sections were stained with fluorescein isothiocyanate (FITC) isomer I (Sigma-Aldrich) to visualize the pericellular space, similar to the methods of Ciani *et al.* [25]. The samples were placed in a rotator (Agar Scientific) with FITC solution at 1 per cent in ethanol and mixed for 4 h at room temperature. The sections were then rinsed in 100 per cent ethanol for 30 min, air-dried and mounted on coverslips using DPX Mounting Media (Sigma-Aldrich). Samples and containers were covered in aluminium foil at all times to prevent photobleaching.

Confocal scans were taken using a confocal microscope (Zeiss LSM 51) with a 40× oil immersion lens, 1.25 numerical aperture, laser wavelength excitation of 488 nm and the pinhole set at 1 Airy unit. All scans were taken at a resolution of 2048 × 2048 pixels giving a field of view of 255 μm. An example of these images can be seen in figure 1*a*,*b*, where lacunae can clearly be seen oriented concentrically around a Haversian canal. A *z*-stack was obtained at increments of 0.41 μm using laser scanning mode through the depth of the section.

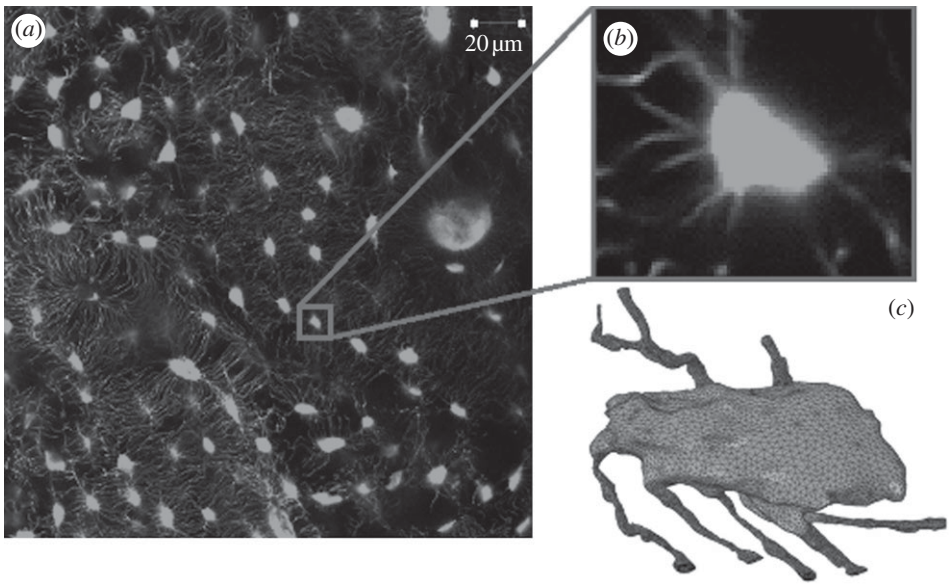

Figure 1. (*a*) Confocal microscopy scan of the lacunar–canalicular network with (*b*) an individual osteocyte and (*c*) a finite element volume mesh of the osteocyte.

2.2. Solid model/mesh generation

Finite element models were constructed of confocal image-derived and idealized cells that included the cell membrane, PCM and the ECM.

2.2.1. Confocal image-derived models

MIMICS, image-processing software, was employed to generate a three-dimensional solid model (Materialise). Confocal image stacks of four osteocyte lacunae were imported into MIMICS and thresholded to between −884 and −769 Hounsfield units. Thresholding allowed segmentation of the lacunar–canalicular space from the surrounding matrix. The lacunar geometries generated were similar to a slightly flattened ellipsoid with major axes ranging between 14 and 16 µm, and minor axes of 8.5–9.5 µm. The canaliculi generated had an average diameter of 0.5–0.7 µm. These models were then meshed using 3-MATIC voxel-meshing software (Materialise). A Boolean subtraction was performed to construct the calcified ECM. In addition, the mesh was offset by 0.08 µm to create a pericellular space and a PCM of the same thickness was constructed by Boolean subtraction. A representative geometry of the ECM, PCM and osteocyte in a confocal image-derived model is shown in figure 2*a*. These geometries were then meshed using four-noded C3D4 tetrahedral elements (figure 1*c*) and exported to ABAQUS finite element software.

The PCM represented the entire space between the ECM and the osteocyte. In order to investigate the strain amplification effect of the PCM, it was removed in some simulations. In these cases the ECM volume was increased to fill this space and contact the cell. These geometries were then meshed using four-noded C3D4 tetrahedral elements.

2.2.2. Idealized model

A solid model of an idealized osteocyte lacuna was developed for comparison using ABAQUS finite element software. The lacuna was modelled as an ellipsoid with minor and major axes equal to 9 and 15 µm, respectively, which were taken as the median dimensions from our confocal scans [26]. The canaliculi were modelled as channels in the ECM with a diameter of 0.6 µm. The osteocyte was also modelled as an ellipsoid with minor and major axes of 7.5 and 13.5 µm, respectively, allowing for a surrounding PCM with a thickness of 0.75 µm [19,27]. The cell processes were created by offsetting from the canaliculi by 0.08 µm [28]. The PCM represented the entire space between the ECM and the osteocyte and in simulations where the PCM is removed to examine the effect of its absence, the ECM is enlarged to fill this space and contact the osteocyte. The geometries of the ECM, PCM and osteocyte are displayed in figure 2*b*. These geometries were then meshed using four-noded C3D4 tetrahedral elements.

2.2.3. Idealized model with extracellular matrix projections

In order to investigate the effect of ECM projections on strain transfer into the osteocyte, an idealized model was developed that included conical ECM protrusions (height of 0.08 µm and base radius 0.1 µm) that projected into the PCM space [28]. The projections were organized in groups of four about the axis of the canaliculi, spaced 1 µm apart along its length (figure 2*c*,*d*). While the distance between adjacent projections has been observed to be approximately 0.1 µm [19], spacing of 1 µm was selected in order to reduce the computing power required and to better observe the localized effects of individual projections.

2.3. Finite element analysis

2.3.1. Material properties and loading

All structures were modelled as linearly elastic, isotropic materials. The viscoelastic nature of the cell was neglected for simplicity as physiological loading of bones occurs at a frequency of approximately 1 Hz, well below the relaxation time of 41.5 s measured in bone cells [29,30]. An

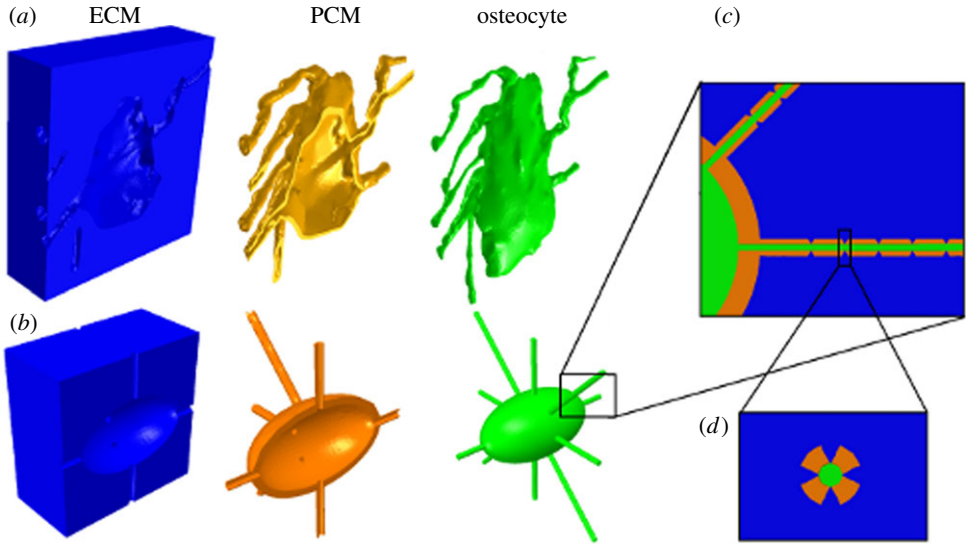

Figure 2. (*a*) Models of confocal image-derived and (*b*) idealized osteocytes depicting extracellular matrix (blue), pericellular matrix (yellow) and osteocyte cell body (green), with ECM projections visible longitudinally in (*c*) and in cross section in (*d*).

elastic modulus of 16 GPa and Poisson's ratio of 0.38 were attributed to the ECM [31]. At present, there is no experimental data available to define the material properties of the PCM surrounding the osteocyte. Therefore, the properties of chondrocyte PCM were assumed, with an elastic modulus of 40 kPa and Poisson's ratio of 0.4 [32,33]. A modulus of 4.47 kPa and Poisson's ratio of 0.3 was attributed to the osteocyte cell body and processes [34]. Tie constraints were applied to attach the PCM to the ECM and osteocyte where direct contact (i.e. no space between the components) occurred at their respective surfaces. Similarly, when ECM projections were included in the idealized model they were also tied directly to the osteocyte cell membrane.

Finite element simulations were conducted to investigate the strain experienced at the cellular level under global loading conditions representing under-loading (500 $\mu\varepsilon$), homeostatic loading (1500 $\mu\varepsilon$) and loading during physical exertion (3000 $\mu\varepsilon$) [5]. A displacement boundary condition was applied to model faces to generate compressive loads of 500, 1500 and 3000 $\mu\varepsilon$ globally. Uniaxial-ramped static loading was applied symmetrically, with opposing faces constrained symmetrically to prevent rigid body motion. In order to examine the effect of anisotropy of the osteocyte, an additional analysis was performed, with the cell assumed to be a transversely isotropic material with a 3 : 1 ratio of in-plane versus out-of-plane stiffness. A strain amplification factor was calculated for each osteocyte as the maximum principal strain in the cell divided by the applied global strain.

3. RESULTS

The finite element contour plots of the confocal image-derived and idealized cell models in figure 3 show the areas of each cell, which experience strain within specific intervals of microstrain, under global applied loading of 3000 $\mu\varepsilon$. Qualitatively, it can be seen from these images that the maximum principal strains are higher in the realistic models (*a–d*) than in the idealized models (*e,f*).

For an applied load of 500 $\mu\varepsilon$, representing low levels of physiological loading, more than 99 per cent of confocal image-derived, and idealized osteocyte volumes experienced strains lower than 1000 $\mu\varepsilon$. Maximum principal strains of 3800–3900 $\mu\varepsilon$ ($\sigma = 3858 \pm 49$ $\mu\varepsilon$) were experienced in the confocal image-derived cells, whereas 1100 $\mu\varepsilon$ was the maximum strain predicted in the idealized model.

Homeostatic physiological loading of 1500 $\mu\varepsilon$ resulted in 2–13% of the volumes of confocal image-derived osteocytes stimulated more than 2000 $\mu\varepsilon$, whereas this figure was just 1 per cent for the idealized model. Maximum principal strains predicted in confocal image-derived osteocytes were 11 000–13 000 $\mu\varepsilon$ ($\sigma = 11\,933 \pm 612$ $\mu\varepsilon$), with 3300 $\mu\varepsilon$ being the maximum strain experienced by the osteocyte in the idealized model. While maximum strains in confocal image-derived models were more than 10 000 $\mu\varepsilon$, these were predicted in a negligible proportion (less than 0.001%) of the models.

For an applied load of 3000 $\mu\varepsilon$, representing vigorous physiological activity, the confocal image-derived models predicted strain values more than 3500 $\mu\varepsilon$ throughout 7–28% of the cell body, whereas only 0.1 per cent of the volume of the idealized osteocytes experienced strain above this level (figure 4). Maximum principal strains predicted in the confocal image-derived osteocytes were 23 000–26 000 $\mu\varepsilon$ ($\sigma = 24\,233 \pm 1033$ $\mu\varepsilon$), compared with a maximum strain of 6600 $\mu\varepsilon$ in the idealized model. The strains observed in the models are used to calculate a strain amplification factor of 7.7–8.9 for the confocal image-derived models. The strain amplification factor for the idealized model without the ECM projections was 2.2. All four confocal image-derived osteocyte models experienced strains greater than 10 000 $\mu\varepsilon$ in approximately 1 per cent of the cell volume when 3000 $\mu\varepsilon$ global loading was applied. However, the idealized model without the projections did not see these strains. In addition a slight decrease in the

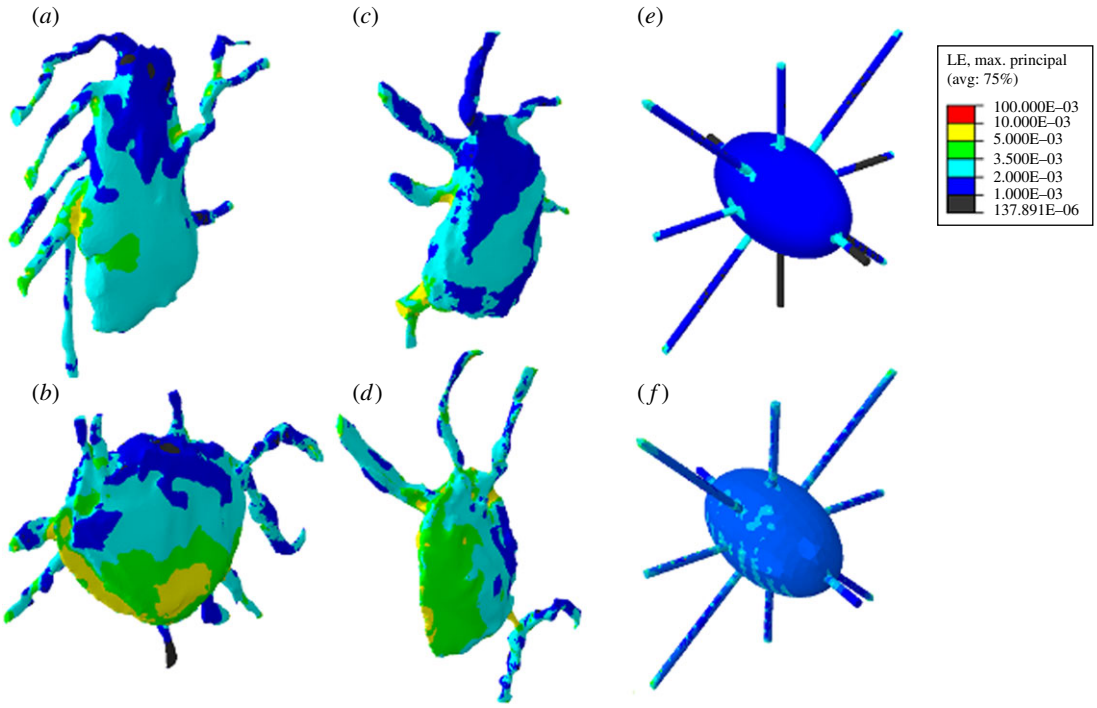

Figure 3. Strain distribution in four confocal image-derived models of osteocytes (*a*–*d*) and idealized osteocytes without extracellular matrix projections (*e*), and with extracellular matrix projections included (*f*) under global loading of 3000 με.

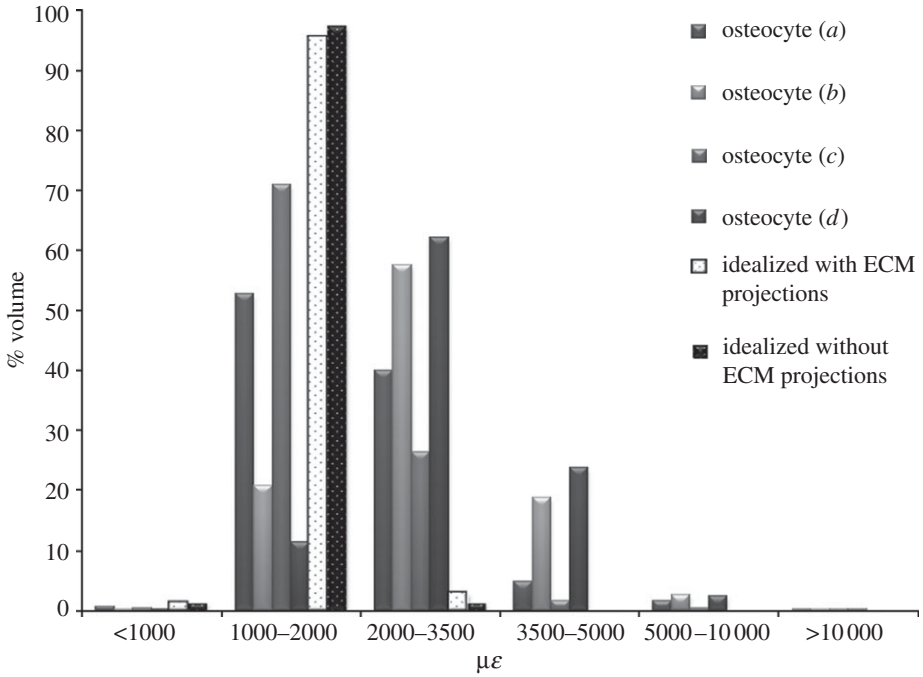

Figure 4. Strain distribution in confocal image-derived (*a*–*d*, as in figure 3) and idealized osteocytes (*e*,*f* in figure 3) under 3000 με compression. Results are shown for idealized models both with and without the ECM projections.

volume of the PCM, of 0.0836–0.1191% ($\sigma = 0.0986 \pm 0.0144\%$), was also observed during loading in all models.

Evidence of the presence of ECM projections was detected in the confocal image-derived models constructed from confocal images, as depicted in figure 5*a*,*b*. Indentations indicating the presence of ECM projections are highlighted, with strain concentrated in these areas on the cell process. Maximum strain levels predicted around these points ranged from 4500 to 5000 με, resulting in amplification of the applied loading by 50–67%. This generated a strain amplification factor of 1.5–1.67. The idealized model that includes the ECM projections (figure 2*f*) shows more concentrated strain in the cell processes than the idealized model without these (figure 2*e*). It can be seen from the graph in figure 4 that in the idealized

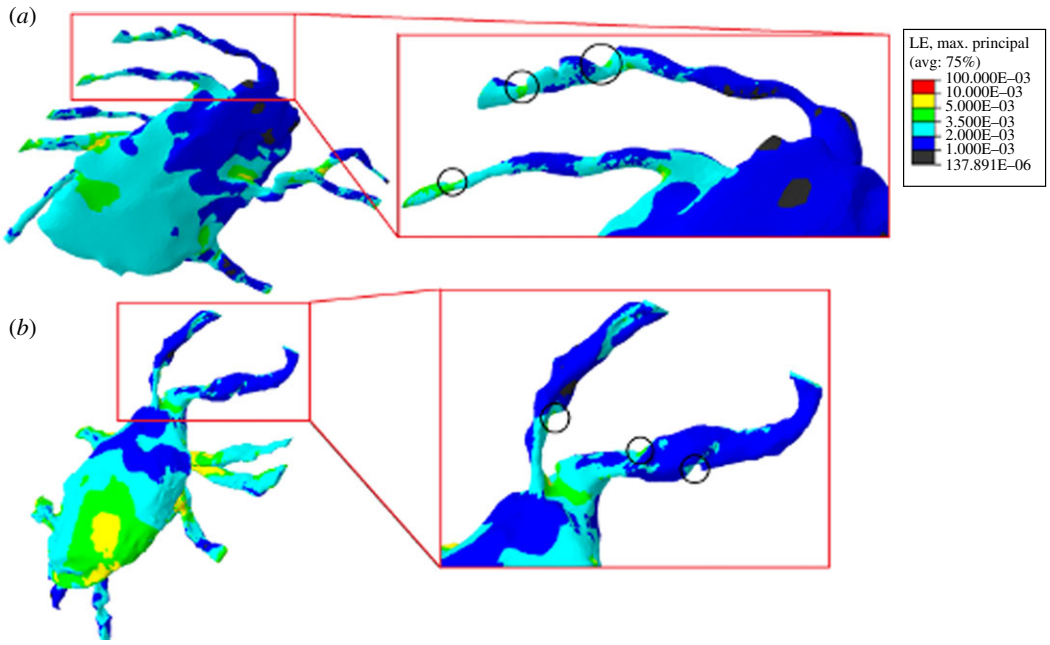

Figure 5. (*a*) Close-up image of confocal image-derived osteocytes and (*b*) loaded at 3000 $\mu\varepsilon$, with indentations circled showing the presence of ECM projections and associated strain concentration.

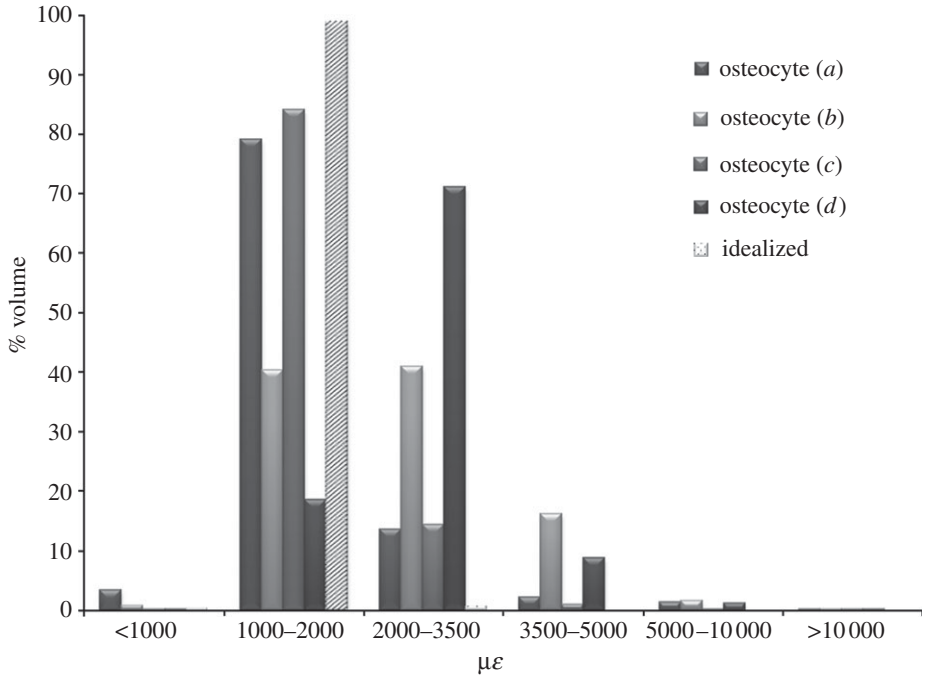

Figure 6. Strain distribution in confocal image-derived (*a*–*d*, as in figure 3) and idealized osteocytes under 3000 $\mu\varepsilon$ compressive loading, without a pericellular matrix.

loading case of 3000 $\mu\varepsilon$, the inclusion of ECM projections resulted in a 0.25 per cent increase in the proportion of the osteocyte experiencing high strain levels (more than 3500 $\mu\varepsilon$). Maximum strains localized around the ECM projections in the idealized model were 6600–12 600 $\mu\varepsilon$, which is 220–420% higher than the applied global loading. This resulted in a strain amplification factor of 4.2 for the model. Simulations of the confocal image-derived and idealized models without a PCM were performed. The results of the 3000 $\mu\varepsilon$ loading case are shown in figure 6. It can be seen that 1–17% of the confocal image-derived models experience strain levels more than 3500 $\mu\varepsilon$, whereas the idealized model senses this strain in less than 0.1 per cent of its volume. Maximum principal strains in the confocal image-derived models without a PCM were found to be 29 000–69 000 $\mu\varepsilon$ ($\sigma = 57\,925 \pm 16\,630\ \mu\varepsilon$), whereas a maximum strain of 7000 $\mu\varepsilon$ was predicted in the idealized model without a PCM. The strain amplification factors for these models were calculated as 9.8–23.3 for the confocal image-derived models and 2.3 for the idealized model.

Furthermore, under applied loading of 3000 με, the transversely isotropic osteocytes experienced maximum principal strains (23 700–29 100 με) which were 3.7–12.2% greater than those predicted in isotropic osteocytes.

4. DISCUSSION

In this study, we developed geometrically accurate three-dimensional computational models of osteocytes in their native environment to study the effects of physiological loading in detail on the mechanical stimuli experienced by the osteocyte. Our results show for the first time that even under strains of 3000 με, 7–28% of the volume of the osteocyte experiences strains in excess of 3500 με, and indeed 1 per cent of an osteocyte volume experiences strains in excess of 10 000 με with maximum principal strains of 23 000–26 000 με. In contrast, elevated strains (more than 3500 με) were predicted only 1 per cent of the idealized model under similar loading conditions, with a maximum principal strain of 6600 με. The strain amplification factor was shown to be 3.5–4 times higher in confocal image-derived models compared with an idealized model. Most notably, while all osteocyte models experienced strains more than 5000 με level that generates some biological response *in vitro*, only the confocal image-derived models predicted maximum strains well more than 10 000 με, which is the approximate strain stimulus necessary to elicit a significant osteogenic response in osteocytes [10]. These findings demonstrate the importance of accurate geometrical modelling when simulating the osteocyte *in vivo* mechanical environment, and the strain amplification effect of the lacunar–canalicular architecture. The results of this study also served to reinforce two theories: (i) the PCM plays an important role in osteocyte mechanical stimulation [35–37] and (ii) ECM projections act to amplify matrix strains at the cell membrane [21].

It must be noted that a number of assumptions were made in the development of these models. Firstly, the ECM, PCM and cell materials were assumed to be linear elastic isotropic materials, and material properties were assumed based on values available for cultured osteocytes and chondrocytes [31–34]. For the purposes of this study, it was impractical to include an advanced material model due to the highly nonlinear nature of the geometry, which resulted in 4.5 million elements and an average computational solving time of 12 h. The mechanical behaviour of osteocytes *in vivo* has not been characterized at this scale, as direct analysis of such a closed biological system has proved unfeasible. Furthermore, the ECM is composed of collagen fibrils and mineral crystals that are intricately organized within this matrix and have been shown to affect stress distribution about the lacuna [38–40]. It would therefore be more appropriate to model the ECM as an anisotropic or transversely isotropic material [41–42]. It should also be noted that the distance between the osteocyte and the ECM was assumed to be constant at 0.08 μm in the confocal imaged-derived models. However, *in vivo* tracer studies and TEM imaging have reported a range of 0.078 ± 0.038 μm [19,27,28] for this spacing. Owing to the experimental challenges of obtaining the precise size of the gap at all locations surrounding the cell body, this assumption was deemed necessary. In reality, certain regions would be in closer proximity to the ECM and at such locations strain transfer to the osteocytes would be increased, as is clearly demonstrated by the results of our idealized ECM projections study.

Furthermore, the cell body and membrane are highly nonlinear materials [43], and the internal actin cytoskeleton in particular plays an integral role in cell mechanics by actively adapting in response to applied mechanical forces [44–46]. An analysis of transversely isotropic cells was performed in order to investigate the effect of anisotropy of the cell on the strain stimulus to its membrane. Our results show that there is a 3.7–12.2% increase in maximum principal strains experienced by a transversely isotropic osteocyte compared with an isotropic model. However, it must be noted that the precise anisotropic behaviour of osteocytes has never been determined. Nonetheless, this analysis reveals that an anisotropic actin cytoskeleton would enhance the strain amplification observed in this study. Future studies should incorporate the active behaviour of the actin cytoskeleton in order to provide more realistic simulations of osteocyte mechanobiology *in vivo* [15]. However, our overall focus was on the role of geometrical changes and based on these studies we expect that the strain amplification effect observed here would be more pronounced if an active actin cytoskeleton and a fluid-saturated PCM were included.

While previous computational research has examined idealized models of the osteocyte mechanical environment in three-dimensional [22,47], this study represents the first development of accurate three-dimensional finite element geometries of the osteocyte, with its canaliculi and surrounding matrix, to predict osteocyte mechanobiology. We report here that the maximum strains predicted in confocal image-derived models are approximately 17 000–20 000 με higher than strains predicted through previous idealized computational approaches [22,47], but are lower than the maximum strains of approximately 35 000 με reported from experimental imaging of lacunae on a two-dimensional exposed plane [11–13]. It must be noted that those experimental studies characterized strain in the lacunae, as opposed to strain measured in the cell [11–13], and also that the authors proposed that microdamage artefacts might be exacerbating local tissue deformation [11–13]. Therefore, it is unlikely that such high strain levels would indeed be experienced by the osteocyte *in vivo*, and our results correlate better with average strains between 7500 and 20 000 με reported in experimental studies [11–13]. Our results demonstrate that the *in vivo* geometrical characteristics of the surrounding ECM and PCM lead to a high degree of strain transfer into the cell body and must be considered for understanding mechanotransduction in osteocytes *in vivo*.

Our studies provide direct evidence that the PCM does indeed act to amplify the strains experienced by the cell membrane, which was previously shown using two-dimensional idealized analytical models of a

transverse section of a canaliculus [15–18,21]. It is interesting to note that in our study we report that the presence of a PCM reduces the maximum strain in confocal image-derived osteocytes by approximately 80 per cent, but that the total volume of the cells stimulated more than 3500 $\mu\varepsilon$ increases by 4–10%. This implies a strain-shielding effect, whereby the PCM absorbs very high strains while also increasing the overall strain transfer to the cell. A similar effect has been predicted in recent computational studies of chondrocytes, which found a wider overall stress distribution despite a decrease of 20–52% in maximum stress values in the cell when a PCM was included [29,33]. In the idealized simulation, maximum strains actually increased by 37 per cent with the inclusion of a PCM, alongside a slight increase in the volume experiencing strain more than 3500 $\mu\varepsilon$. This may be explained by the simplified geometry of the idealized model resulting in poor strain amplification in the absence of a PCM. These results emphasize the important role that the PCM plays in osteocyte strain sensing and mechanotransduction. The PCM has a low elastic modulus and deforms significantly under compression compared with the calcified ECM, resulting in high strain transfer to the osteocyte cell membrane.

It should be noted that *in vivo* the PCM consists of jelly-like glycocalyx, and the interstitial fluid within this matrix is capable of flowing through the lacunar–canalicular network under mechanical loading of the ECM. Analytical models developed by Weinbaum *et al.* [15–18,21] represented the PCM as matrix of fibres, which tethered the cell process to the canalicular wall, and incorporated interstitial fluid drag forces under mechanical loading. These studies suggested that the stimulus arising from loading-induced fluid flow plays an important role in osteocyte mechanobiology. Computational fluid dynamics has also shown that fluid flow characteristics within osteocyte canaliculi have a profound effect on shear stress experienced by cell processes [23]. While fluid dynamics were not incorporated into our models, we predict a decrease in the volume of the PCM (approx. 0.1%) and propose that, owing to such volumetric changes under mechanical loading, fluid flow would indeed occur and might provide an additional stimulus to the cell. Future studies of the fluid flow within this matrix under the observed volume change reported here would provide a unique insight into mechanical stimulation of bone cells under matrix strain- and loading-induced fluid flow *in vivo*.

It is interesting that we observe evidence of projections of the ECM into the pericellular space in our confocal image-derived geometries, which were first identified using TEM imaging [19]. Localized strain amplification appears to occur around these ECM projections, magnifying the applied strain by 50–67%. When these projections were incorporated into the idealized model local strain amplification of 220–420% of global strain was predicted, increasing the strain amplification factor of the overall model by 190 per cent. These findings highlight the ability of ECM projections to act as powerful strain amplification mechanisms in osteocyte mechanobiology, particularly owing to their location in the most mechanosensitive region of the cell [20]. Furthermore, the spacing between adjacent projections was increased from 0.1 to 1 μm to reduce the large computational power required for the simulations. Employing a spacing of 0.1 μm would result in the presence of many more projections, which would in turn impart even greater strain stimulus to the osteocyte.

Of particular interest is the loading case representing vigorous physiological activity (3000 $\mu\varepsilon$) as it is under this level of global mechanical loading that appreciable strain more than 10 000 $\mu\varepsilon$ is observed in the osteocyte. This is significant as previous *in vitro* studies have shown that strain levels above approximately 10 000 $\mu\varepsilon$ result in elevated levels of intracellular cytosolic calcium mobilization (Ca_i^{2+}) and alkaline phosphatase (ALP) in cultured osteocyte-like cells [9,48]. As Ca_i^{2+} mobilization is an early intracellular signalling event involved in bone mechanotransduction, and ALP is a marker for bone mineralization and ECM deposition, these are good indicators of the anabolic effect of mechanical stimulus. Past studies applying large strains (more than 10 000 $\mu\varepsilon$) have also observed increased nitric oxide (NO) and prostaglandin (PG) production, both essential for an osteogenic response, at these strain levels [49,50]. In contrast, more recent studies have suggested that production of NO and PGs, as well as mRNA expression of the important bone remodelling protein osteopontin, may be more closely linked with loading-induced fluid flow than direct substrate stimulation [9,48,51]. However, these studies did not investigate direct mechanical loading more than 5000 $\mu\varepsilon$. Therefore, it is possible that the elevated strain levels (more than 10 000 $\mu\varepsilon$) predicted in our models and previous experimental studies [11–13] may also stimulate these biochemical osteogenic responses, particularly owing to the strain amplification effects of the PCM and ECM projections.

5. CONCLUSION

In this study, we report that confocal image-derived models subjected to physiologically active loading levels (3000 $\mu\varepsilon$) predict 350–400% greater strain amplification experienced by osteocytes compared with an idealized cell. Furthermore, we predict that the PCM increases the cell volume stimulated more than 3500 $\mu\varepsilon$ by 4–10% and that ECM projections amplify strain to the cell by approximately 50–420%. In addition, decreases in the volume of this matrix were also predicted, suggesting the occurrence of mechanically driven interstitial fluid flow. These are the first confocal image-derived computational models of osteocytes *in vivo* and provide a greater understanding of the mechanical environment of the osteocyte.

The authors acknowledge funding from the Irish Research Council for Science, Engineering and Technology, under the EMBARK programme (S.W.V.), the European Research Council (ERC) under grant no. 258992 (BONEMECHBIO) and the Irish Centre for High-End Computing (ICHEC).

REFERENCES

1 Haj, A. J. E., Minter, S. L., Rawlinson, S. C. F., Suswillo, R. & Lanyon, L. E. 1990 Cellular responses to mechanical loading

in vitro. *J. Bone Mineral Res.* **5**, 923–932. (doi:10.1002/jbmr.5650050905)
2 Che, J.-H., Liu, C., You, L. & Simmons, C. A. 2010 Boning up on Wolff's law: mechanical regulation of the cells that make and maintain bone. *J. Biomech.* **43**, 108–118. (doi:10.1016/j.jbiomech.2009.09.016)
3 Sittichockechaiwut, A., Scutt, A. M., Ryan, A. J., Bonewald, L. F. & Reilly, G. C. 2009 Use of rapidly mineralising osteoblasts and short periods of mechanical loading to accelerate matrix maturation in 3D scaffolds. *Bone* **44**, 822–829. (doi:10.1016/j.bone.2008.12.027)
4 McMahon, L., Reid, A., Campbell, V. & Prendergast, P. 2008 Regulatory effects of mechanical strain on the chondrogenic differentiation of MSCs in a collagen-GAG scaffold: experimental and computational analysis. *Ann. Biomed. Eng.* **36**, 185–194. (doi:10.1007/s10439-007-9416-5)
5 Burr, D. B., Milgrom, C., Fyhrie, D., Forwood, M., Nyska, M., Finestone, A., Hoshaw, S., Saiag, E. & Simkin, A. 1996 *In vivo* measurement of human tibial strains during vigorous activity. *Bone* **18**, 405–410. (doi:10.1016/8756-3282(96)00028-2)
6 Fritton, S. P., Kenneth, J. M. & Rubin, C. T. 2000 Quantifying the strain history of bone: spatial uniformity and self-similarity of low-magnitude strains. *J. Biomech.* **33**, 317–325. (doi:10.1016/S0021-9290(99)00210-9)
7 Carter, D. R., Fyhrie, D. P. & Whalen, R. T. 1987 Trabecular bone density and loading history: regulation of connective tissue biology by mechanical energy. *J. Biomech.* **20**, 785–794. (doi:10.1016/0021-9290(87) 90058-3)
8 Mosley, J. R. 2000 Osteoporosis and bone functional adaptation: mechanobiological regulation of bone architecture in growing and adult bone, a review. *J. Rehabil. Res. Dev.* **37**, 189–199.
9 You, J., Yellowley, C. E., Donahue, H. J., Zhang, Y., Chen, Q. & Jacobs, C. R. 2000 Substrate deformation levels associated with routine physical activity are less stimulatory to bone cells relative to loading-induced oscillatory fluid flow. *J. Biomech. Eng.* **122**, 387–393. (doi:10.1115/1.1287161)
10 Burger, E. H. & Veldhuijzen, J. P. 1993 Influence of mechanical factors on bone formation, resorption and growth *in vitro*. *Bone* **7**, 37–56.
11 Nicolella, D. P., Bonewald, L. F., Moravits, D. E. & Lankford, J. 2005 Measurement of microstructural strain in cortical bone. *Eur. J. Morphol.* **42**, 23–29. (doi:10.1080/09243860500095364)
12 Nicolella, D. P., Moravits, D. E., Gale, A. M., Bonewald, L. F. & Lankford, J. 2006 Osteocyte lacunae tissue strain in cortical bone. *J. Biomech.* **39**, 1735–1743. (doi:10.1016/j.jbiomech.2005.04.032)
13 Nicolella, D. P., Nicholls, A. E., Lankford, J. & Davy, D. T. 2001 Machine vision photogrammetry: a technique for measurement of microstructural strain in cortical bone. *J. Biomech.* **34**, 135–139. (doi:10.1016/S0021-9290(00)00163-9)
14 Schneider, P., Meier, M., Wepf, R. & Müller, R. 2010 Towards quantitative 3D imaging of the osteocyte lacuno-canalicular network. *Bone* **47** 848–858. (doi:10.1016/j.bone.2010.07.026)
15 Han, Y., Cowin, S. C., Schaffler, M. B. & Weinbaum, S. 2004 Mechanotransduction and strain amplification in osteocyte cell processes. *Proc. Natl Acad. Sci. USA* **101**, 16 689–16 694. (doi:10.1073/pnas.0407429101)
16 Weinbaum, S., Cowin, S. C. & Zeng, Y. 1994 A model for the excitation of osteocytes by mechanical loading-induced bone fluid shear stresses. *J. Biomech.* **27**, 339–360. (doi:10.1016/0021-9290(94)90010-8)
17 You, L., Cowin, S. C., Schaffler, M. B. & Weinbaum, S. 2001 A model for strain amplification in the actin cytoskeleton of osteocytes due to fluid drag on pericellular matrix. *J. Biomech.* **34**, 1375–1386. (doi:10.1016/S0021-9290(01)00107-5)
18 Zeng, Y., Cowin, S. & Weinbaum, S. 1994 A fiber matrix model for fluid flow and streaming potentials in the canaliculi of an osteon. *Ann. Biomed. Eng.* **22**, 280–292. (doi:10.1007/bf02368235)
19 McNamara, L. M., Majeska, R. J., Weinbaum, S., Friedrich, V. & Schaffler, M. B. 2009 Attachment of osteocyte cell processes to the bone matrix. *Anat. Record: Adv. Integr. Anat. Evol. Biol.* **292**, 355–363. (doi:10.1002/ar.20869)
20 Adachi, T., Aonuma, Y., Tanaka, M., Hojo, M., Takano-Yamamoto, T. & Kamioka, H. 2009 Calcium response in single osteocytes to locally applied mechanical stimulus: differences in cell process and cell body. *J. Biomech.* **42**, 1989–1995. (doi:10.1016/j.jbiomech.2009.04.034)
21 Wang, Y., McNamara, L. M., Schaffler, M. B. & Weinbaum, S. 2007 A model for the role of integrins in flow induced mechanotransduction in osteocytes. *Proc. Natl Acad. Sci. USA* **104**, 15 941–15 946. (doi:10.1073/pnas.0707246104)
22 Rath Bonivtch, A., Bonewald, L. F. & Nicolella, D. P. 2007 Tissue strain amplification at the osteocyte lacuna: a microstructural finite element analysis. *J. Biomech.* **40**, 2199–2206. (doi:10.1016/j.jbiomech.2006.10.040)
23 Anderson, E. J. & Knothe Tate, M. L. 2008 Idealization of pericellular fluid space geometry and dimension results in a profound underprediction of nano-microscale stresses imparted by fluid drag on osteocytes. *J. Biomech.* **41**, 1736–1746. (doi:10.1016/j.jbiomech.2008.02.035)
24 McCreadie, B. R., Hollister, S. J., Schaffler, M. B. & Goldstein, S. A. 2004 Osteocyte lacuna size and shape in women with and without osteoporotic fracture. *J. Biomech.* **37**, 563–572. (doi:10.1016/S0021-9290(03) 00287-2)
25 Ciani, C., Doty, S. B. & Fritton, S. P. 2009 An effective histological staining process to visualize bone interstitial fluid space using confocal microscopy. *Bone* **44**, 1015–1017. (doi:10.1016/j.bone.2009.01.376)
26 Lin, Y. & Xu, S. 2011 AFM analysis of the lacunar–canalicular network in demineralized compact bone. *J. Microsc.* **241**, 291–302. (doi:10.1111/j.1365-2818.2010.03431.x)
27 You, L-D., Weinbaum, S., Cowin, S. C. & Schaffler, M. B. 2004 Ultrastructure of the osteocyte process and its pericellular matrix. *Anat. Rec. A. Discov. Mol. Cell. Evol. Biol.* **278A**, 505–513. (doi:10.1002/ar.a.20050)
28 Wang, L., Wang, Y., Han, Y., Henderson, S. C., Majeska, R. J., Weinbaum, S. & Schaffler, M. B. 2005 *In situ* measurement of solute transport in the bone lacunar–canalicular system. *Proc. Natl Acad. Sci. USA* **102**, 11 911–11 916. (doi:10.1073/pnas.0505193102)
29 Appelman, T. P., Mizrahi, J. & Seliktar, D. 2011 A finite element model of cell–matrix interactions to study the differential effect of scaffold composition on chondrogenic response to mechanical stimulation. *J. Biomech. Eng.* **133**, 041 010–041 012. (doi:10.1115/1.4003314)
30 Darling, E. M., Topel, M., Zauscher, S., Vail, T. P. & Guilak, F. 2008 Viscoelastic properties of human mesenchymally-derived stem cells and primary osteoblasts, chondrocytes, and adipocytes. *J. Biomech.* **41**, 454–464. (doi:10.1016/j.jbiomech.2007.06.019)
31 Deligianni, D. & Apostolopoulos, C. 2008 Multilevel finite element modeling for the prediction of local cellular deformation in bone. *Biomech. Model. Mechanobiol.* **7**, 151–159. (doi:10.1007/s10237-007-0082-1)

32 Alexopoulos, L. G., Haider, M. A., Vail, T. P. & Guilak, F. 2003 Alterations in the mechanical properties of the human chondrocyte pericellular matrix with osteoarthritis. *J. Biomech. Eng.* **125**, 323–333. (doi:10.1115/1.1579047)

33 Alexopoulos, L. G., Setton, L. A. & Guilak, F. 2005 The biomechanical role of the chondrocyte pericellular matrix in articular cartilage. *Acta Biomater.* **1**, 317–325. (doi:10.1016/j.actbio.2005.02.001)

34 Sugawara, Y. *et al.* 2008 The alteration of a mechanical property of bone cells during the process of changing from osteoblasts to osteocytes. *Bone* **43**, 19–24. (doi:10.1016/j.bone.2008.02.020)

35 Burra, S., Nicolella, D. P., Francis, W. L., Freitas, C. J., Mueschke, N. J., Poole, K. & Jiang,, J. X. 2010 Dendritic processes of osteocytes are mechanotransducers that induce the opening of hemichannels. *Proc. Natl Acad. Sci. USA* **107**, 13 648–13 653. (doi:10.1073/pnas.1009382107)

36 Burra, S., Nicolella, D. P. & Jiang, J. X. 2011 Dark horse in osteocyte biology: glycocalyx around the dendrites is critical for osteocyte mechanosensing. *Commun. Integr. Biol.* **4**, 48–50. (doi:10.4161/cib.4.1.13646)

37 Reilly, C. G., Haut, R. T., Yellowley, E. C., Donahue, J. H. & Jacobs, R. C. 2003 Fluid flow induced PGE2 release by bone cells is reduced by glycocalyx degradation whereas calcium signals are not. *Biorheology* **40**, 591–603.

38 Currey, J. D. 2003 The many adaptations of bone. *J. Biomech.* **36**, 1487–1495. (doi:10.1016/S0021-9290(03)00124-6)

39 Ascenzi, M-G., Gill, J. & Lomovtsev, A. 2008 Orientation of collagen at the osteocyte lacunae in human secondary osteons. *J. Biomech.* **41**, 3426–3435. (doi:10.1016/j.jbiomech.2008.09.010)

40 Hofmann, T., Heyroth, F., Meinhard, H., Fränzel, W. & Raum, K. 2006 Assessment of composition and anisotropic elastic properties of secondary osteon lamellae. *J. Biomech.* **39**, 2282–2294. (doi:10.1016/j.jbiomech.2005.07.009)

41 Neil Dong, X. & Edward Guo, X. 2004 The dependence of transversely isotropic elasticity of human femoral cortical bone on porosity. *J. Biomech.* **37**, 1281–1287. (doi:10.1016/j.jbiomech.2003.12.011)

42 O'Mahony, A. M., Williams, J. L. & Spencer, P. 2001 Anisotropic elasticity of cortical and cancellous bone in the posterior mandible increases peri-implant stress and strain under oblique loading. *Clin. Oral Implants Res.* **12**, 648–657. (doi:10.1034/j.1600-0501.2001.120614.x)

43 Lim, C. T., Zhou, E. H. & Quek, S. T. 2006 Mechanical models for living cells: a review. *J. Biomech.* **39**, 195–216. (doi:10.1016/j.jbiomech.2004.12.008)

44 Ofek, G., Dowling, E., Raphael, R., McGarry, J. & Athanasiou, K. 2010 Biomechanics of single chondrocytes under direct shear. *Biomech. Model Mechanobiol.* **9**, 153–162. (doi:10.1007/s10237-009-0166-1)

45 McGarry, J. P., Fu, J., Yang, M. T., Chen, C. S., McMeeking, R. M., Evans, A. G. & Deshpande, V. S. 2009 Simulation of the contractile response of cells on an array of micro-posts. *Phil. Trans. R. Soc. A* **367**, 3477–3497. (doi:10.1098/rsta.2009.0097)

46 McGarry, J. 2009 Characterization of cell mechanical properties by computational modeling of parallel plate compression. *Ann. Biomed. Eng.* **37**, 2317–2325. (doi:10.1007/s10439-009-9772-4)

47 McCreadie, B. R. & Hollister, S. J. 1997 Strain concentrations surrounding an ellipsoid model of lacunae and osteocytes. *Comput. Methods Biomech. Biomed. Eng.* **1**, 61–68. (doi:10.1080/01495739708936695)

48 Smalt, R., Mitchell, F. T., Howard, R. L. & Chambers, T. J. 1997 Induction of NO and prostaglandin E2 in osteoblasts by wall-shear stress but not mechanical strain. *Am. J. Physiol. Endocrinol. Metab.* **273**, E751–E8.

49 Pitsillides, A., Rawlinson, S., Suswillo, R., Bourrin, S., Zaman, G. & Lanyon, L. 1995 Mechanical strain-induced NO production by bone cells: a possible role in adaptive bone (re)modeling? *FASEB J.* **9**, 1614–1622.

50 Yeh, C-K. & Rodan, G. 1984 Tensile forces enhance prostaglandin E synthesis in osteoblastic cells grown on collagen ribbons. *Calcif. Tissue Int.* **36**, S67–S71. (doi:10.1007/bf02406136)

51 Owan, I., Burr, D. B., Turner, C. H., Qiu, J., Tu, Y., Onyia, J. E. & Duncan, R. L. 1997 Mechanotransduction in bone: osteoblasts are more responsive to fluid forces than mechanical strain. *Am. J. Physiol. Cell Physiol.* **273**, C810–C815.